Enhanced Relaxometric Properties of MRI "Positive" Contrast Agents Confined in Three-Dimensional Cubic Mesoporous Silica Nanoparticles

ARTICLE *in* ADVANCED FUNCTIONAL MATERIALS · DECEMBER 2011

Impact Factor: 11.81 · DOI: 10.1002/adfm.201101766

5 AUTHORS, INCLUDING:

Remy Guillet-Nicolas
Quantachrome Instruments
19 PUBLICATIONS **295** CITATIONS
SEE PROFILE

Yongbeom Seo
Institute for Basic Science
20 PUBLICATIONS **577** CITATIONS
SEE PROFILE

Marc-André Fortin
Laval University
33 PUBLICATIONS **501** CITATIONS
SEE PROFILE

Freddy Kleitz
Laval University
125 PUBLICATIONS **4,481** CITATIONS
SEE PROFILE

Enhanced Relaxometric Properties of MRI "Positive" Contrast Agents Confined in Three-Dimensional Cubic Mesoporous Silica Nanoparticles

Rémy Guillet-Nicolas, Jean-Luc Bridot, Yongbeom Seo, Marc-André Fortin, and Freddy Kleitz**

Mesoporous silica nanoparticles (MSNs) are of growing interest for the development of novel probes enabling efficient tracking of cells in vivo using magnetic resonance imaging (MRI). The incorporation of Gd^{3+} paramagnetic ions into highly porous MSNs is a powerful strategy to synthesize "positive" MRI contrast agents for more quantitative T_1-weighted MR imaging. Within this context, different strategies have been reported to integrate Gd chelates to 2D pore network MSNs. As an alternative, we report on the modulation of the pore network topology through the preparation of a 3D pore network hybrid $GdSi_xO_y$ MSN system. In this study, 2D $GdSi_xO_y$-MSNs with similar porosity and particle size were also prepared and the relaxometric performances of both materials, directly compared. Both syntheses lead to water-dispersible MSNs suspensions (particle size < 200 nm), which were stable for at least 48h. 3D $GdSi_xO_y$-MSNs provided a significant increase in ^1H longitudinal relaxivity (18.5 $s^{-1}mM^{-1}$; 4.6 times higher than Gd-DTPA) and low r_2/r_1 ratios (1.56) compatible with the requirements of "positive" contrast agents for MRI. These results demonstrate the superiority of a 3D pore network to host paramagnetic atoms for MRI signal enhancement using T_1-weighted imaging. Such an approach minimizes the total amount of paramagnetic element per particle.

1. Introduction

Progress in gene therapy, stem cell research and cell transplants for regenerative medicine calls for the development of cellular probes allowing for efficient and high-resolution tracking of cells in vivo using magnetic resonance imaging (MRI). This modality, one of the most widely used in clinical medicine and pre-clinical research, is based on the excitation of ^1H protons in a hydrated tissue. It uses a finely tuned radiofrequency wave to provide whole-body images of a resolution as high as 300 micrometers. The detected signal results from ^1H proton relaxation mechanisms. Paramagnetic metal cations (e.g., Gd^{3+}, Fe^{3+}, Mn^{2+}) are used as chelated compounds, or nanometric constructs, to accelerate the longitudinal relaxation of ^1H protons. Ingested into cells, these paramagnetic elements act as efficient MRI signal enhancers.

To establish MRI as a key imaging modality for cell tracking studies, it is necessary to develop a new generation of high-sensitivity MRI contrast agents that could allow for the efficient detection of labeled cells in vivo. At the moment, Fe-containing nanoparticles are being used as cellular probes, coupled with T_2^*/T_2-weighted imaging sequences. They provide a very sensitive "negative" contrast effect, which enables single cell detection.[1] However the strong magnetic susceptibility of iron oxide nanoparticles induces a negative contrast effect that greatly exceeds the exact area where implanted cells are located. Moreover, these artifacts impede the delineation of fine vasculature and anatomical features around the labeled cells, and make impossible cell quantification based on contrast enhancement. On the other hand, T_1-weighted sequences generally provide images of higher resolution and signal-to-noise ratio than T_2^*/T_2-weighted

R. Guillet-Nicolas, Dr. J.-L Bridot, Prof. F. Kleitz
Department of Chemistry
Université Laval
G1V0A6, Québec, Canada and Centre de Recherche sur les Matériaux Avancés (CERMA), Université Laval, Canada
Fax: (+) 1 418 656 7916
E-mail: freddy.kleitz@chm.ulaval.ca

R. Guillet-Nicolas, Dr. J.-L. Bridot, Prof. M.-A. Fortin
Centre Hospitalier Universitaire de Québec Axe Métabolisme, Santé Vasculaire et Rénale (AMSVR-CHUQ)
Department of Mining, Metallurgy and Materials Engineering, Université Laval,
G1V 0A6, Québec, Canada and Centre de Recherche sur les Matériaux Avancés (CERMA), Université Laval, Canada
Fax: (+) 1 418 525 4372
E-mail: marc-andre.fortin@gmn.ulaval.ca

Y. Seo
Center for Functional Nanomaterials, Department of Chemistry and Graduate School of Nanoscience and Technology (WCU)
Korea Advanced Institute of Science and Technology
Daejeon 305-701, Republic of Korea

DOI: 10.1002/adfm.201101766

ones, and are free of the image artifacts characteristic of high susceptibility materials. Current vascular contrast enhancement procedures with MRI are being performed with paramagnetic molecules based on chelated Gd (i.e., Gd-DTPA, Gd-DOTA, etc.).[2] However, these substances are not efficiently ingested and retained into cells and they do not express high relaxivities per unit of contrast agent. In order to reach nanomolar detection thresholds, a necessary condition to allow for quantitative cell imaging and tracking at higher resolution, new paramagnetic agents for "positive contrast" imaging must be developed. They must contain high concentrations of paramagnetic ions, each one leading to an optimal relaxivity effect on ^{1}H protons diffusing nearby.

Mesoporous silica nanoparticles (MSNs) are being introduced as a biocompatible material to label and track cells with magnetic resonance imaging (MRI).[3–8] The incorporation of Gd^{3+} paramagnetic lanthanide ions into highly porous MSNs is a powerful strategy to develop an efficient "positive" contrast agent for MRI procedures. Indeed, some early works confirmed the safe use of Gd-MSNs for in vivo cell tracking.[4,6a,6b,6d] Taylor et al., for instance, have successfully internalized Gd chelates-containing MSNs into monocyte cells.[4] However, the achieved r_2/r_1 ratios, a value which determinates the efficiency of a positive contrast agent, were far from unity ($2 < r_2/r_1 < 10$). Similarly, Mou et al. reported systems involving MSNs[6] functionalized with Gd complexes, showing adequate cellular internalization properties and positive contrast when observed at clinical field strength (1.5 T) and with T_1 -weighted MRI sequences. High r_1 and r_2 values (23 and 34 $s^{-1}mM^{-1}$, respectively, for the highest values), as well as a r_2/r_1 ratio reaching 1.5, were obtained.

For T_1-weighted applications, relaxometric ratios close to 1 are expected to provide optimal results, and the occurrence of T_2 and T_2^* effects, related to coarse crystals or to the use of high magnetic fields (>3 T), must be avoided. The presence of a significant molar fraction of paramagnetic ions is a determining factor guiding the relaxometric properties of a Gd-based contrast agent. The second very important aspect is the achievement of an optimal contact between Gd^{3+} and water molecules, in order to enhance the relaxivity (r_1), i.e., the ^{1}H relaxation rate normalized to the amount of Gd in the solution. Within this context, Botta's group recently reported a strategy to increase the efficiency of Gd chelates grafted inside MSNs exhibiting a two-dimensional (2D) pore network.[7b] An alternative approach consists in modulating the nature of the porous host platform, i.e., the morphology of the pore network. Indeed, it appears that such materials with 2D porosity could present some limitations as revealed by Carniato et al. who studied Gd-DOTA complexes grafted into 2D MSNs and their resulting influence on pore accessibility.[7a] In addition, materials consisting of a fully interconnected three-dimensional (3D) pore network, i.e., MCM-48-type, could facilitate mass transport processes.[9] Therefore, in these systems, open pore network, higher surface area and large pore volume, together with enhanced permeability to water, could be crucial attributes for producing Gd-MSNs with adequate molar ^{1}H relaxivities.

In this contribution, we report on the preparation of highly porous hybrid $GdSi_xO_y$-MSNs characterized by a 3D pore structure (cubic *Ia3d* mesostructure). $GdSi_xO_y$-MSNs with bidimensional pore structure of similar features (e.g., porosity and particle size) were also prepared and the relaxometric performances of both materials were compared. Aqueous suspensions containing our "3D" $GdSi_xO_y$-MSNs, provide a significant increase in the ^{1}H longitudinal relaxation rate (T_1). Thus, our investigations establish that MSNs used as T_1 contrast agents, should be based on a 3D pore network in order to reach optimal ^{1}H relaxation efficiencies. Furthermore, by using such a strategy, the amount of Gd units per particle could be enhanced, resulting in higher detection sensitivity per particle.

2. Results and discussion

2.1. MSNs Synthesis and Characterization

In general, MSNs are considered biocompatible and are well ingested and tolerated by a wide variety of cells.[8,10–15] However, the size and the shape of the silica particles must be carefully controlled for efficient cell labeling. Optimal cell internalization rates have been achieved with spherical nanoparticles of diameters between 100 and 400 nm.[3,6d,6e,10,11,16,17] In the present study, two MSN systems synthesized in alkaline media and exhibiting almost similar physicochemical properties, i.e., particle size (<200 nm) and pore diameter (<4 nm), were selected as hosts for the Gd^{3+} species. They are designated in the text as NSMCM-48 for the 3D pore network particulate system, and NSMCM-41 for the 2D pore network system (See Experimental Section). A detailed inspection of the 3D NSMCM-48 particles with transmission electron microscopy (TEM) revealed non-aggregated, well-defined and uniform spherical particles, with an average particle size of ~140 nm (**Figure 1**, Figures S1 and S2 in Supporting Information). Analysis of the 2D NSMCM-41 particles revealed similar features (spheroid shape and narrow size distribution) with a mean particle size slightly lower (~110 nm). Both pore networks showed excellent mesoscopic order. The NSMCM-48 particles exhibit 3D cubic *Ia3d* mesopore structure,[18] whereas the pore structure of the NSMCM-41 particles is a linear hexagonal array of channels.[10a] Low-angle powder X-ray diffraction (XRD) data presented in Figure S3 confirmed the respective mesostructure of both materials. Also, both silica materials showed typical nitrogen sorption behavior characteristic of highly ordered mesoporous materials with cylindrical-like pores (**Figure 2**). Whereas similar mesopore diameter values were achieved for the 3D and 2D systems (3.4 and 3.8 nm, respectively), their specific surface areas (1601 and 1274 m^2g^{-1}) and total pore volumes (1.2 and 1.0 cm^3g^{-1}) were noticeably different, i.e., about 20% higher for the 3D cubic mesostructure (see **Table 1**).

2.2. $GdSi_xO_y$-MSN Materials

Large Gd complexes inserted in the small pores of MCM-41 MSN systems (<3–4 nm),[7a] can drastically reduce the diffusion of water molecules into the core of the particles. As a consequence, the contact of Gd with diffusing ^{1}H protons is often impeded. This, in turn, affects the reduction of T_1, and

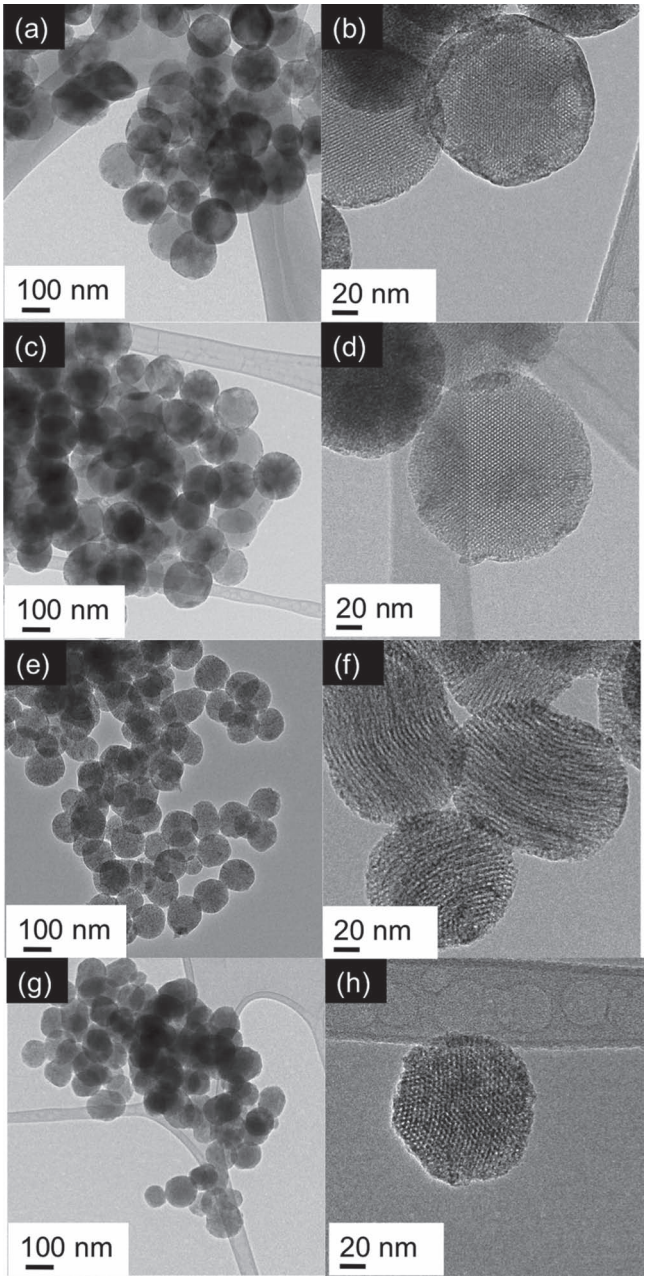

Figure 1. HRTEM images of Gd(2)-NSMCM-48, a,b); Gd(5)-NSMCM-48, c,d); Gd(2)-NSMCM-41, e,f); and Gd(5)-NSMCM-41, g,h).

attenuates the overall efficiency of the positive contrast agent. The aim of the present study was to compare the relaxometric properties of 2D and 3D networks. Because pore obstruction by large Gd complexes could introduce a significant variability in the relaxometric results, possibly impeding a straightforward comparison of the two porous networks, in this study we selected a different mode of insertion: the mesoporous silica framework was impregnated with Gd^{3+} ions (by the incipient wetness technique) using a solution of $Gd(NO_3)_3.6H_2O$ (1, 2 and 5 mmol, per gram of dry silica, in ethanol). After drying, the particles were calcined at 700 °C under air to produce stable $GdSi_xO_y$-MSNs. Upon TEM inspection of the thermally-treated Gd-loaded samples (Figure 1 and **Figure 3**, Figure S2), no obvious change in particle size or any particle aggregation was observed. Moreover, no large Gd_2O_3 crystals were observed outside the silica particles or at their external surface. The absence of wide-angle XRD peaks characteristics of Gd_2O_3 or any $GdSi_xO_y$ crystalline structure, suggests a very fine size for crystalline Gd-containing domains, too small for being discriminated by XRD (Figure S3). Similar results were reported by Huang et al. in the case of materials consisting of gadolinium silicate nanoshells.[19] For both 3D and 2D Gd-loaded networks, nitrogen sorption confirmed a progressive decrease in specific surface area, in pore volume, and in pore size, with increasing Gd loading (Table 1, Figure 2). This is an indication of partial pore filling by Gd; however, the pore volume values remain relatively high, and there is no obvious indication of severe pore obstruction (Table 1).

A confirmation of the Gd distribution inside the mesoporous spheres, was obtained by advanced EDX analyses (performed on high angle annular dark field images, **Figure 4**) for both Gd(5)-NSMCM-48 and Gd(5)-NSMCM-41. These results clearly indicate a successful sequestration of Gd atoms inside the silica porous network after calcination at 700 °C. In both systems, gadolinium seems to be uniformly dispersed inside the porous network of the materials. Similar observations were made at lower loadings, e.g., Gd(2)-NSMCM-48 and Gd(2)-NSMCM-41. Gadolinium was not detected by EDX outside of the MSNs porous framework, which is in perfect agreement with the conclusions extracted from XRD, TEM and N_2 physisorption analyses.

X-ray photoelectron spectroscopy (XPS) analyses were performed with Gd(0, 5)-NSMCM-41,48 samples, with emphasis on O (1s), Si (2p) and Gd (4d) peaks, as shown in **Figure 5**. Both pristine silica structures did reveal only one O (1s), and one Si (2p) peak, at binding energies 533.2–533.1 and 103.8–103.7 eV, respectively. Oxygen-to-silica ratios (O/Si) were 2.62 and 2.77 for the 3D and 2D structures, respectively (Figure 5, Tables S1 and S2). This contribution can be attributed to the Si-O-Si siloxane bonds.[20a] As expected, Gd is present in all Gd(1,2,5)-NSMCM-41,48 samples (Table S2); however, the complexity of the Gd (4d) peak impedes a fine identification of the different chemical binding states for this element. For the silica peak however, both 103.8 eV and 102.1 eV binding energies were observed, indicative of the Si-O-Si and Si-O-Gd links, respectively. Both components also appeared on the O (1s) peaks: 533.2 eV (Si-O-Si) and 531.3 eV (Si-O-Gd) (Table S1).[20a,20b] These results suggest the presence of gadolinium silicate domains, e.g., $GdSi_xO_y$ layers inside the MSNs pores as schematically represented in Figure 3. A triple O (1s) peak would have revealed the presence of ultrafine Gd_2O_3, which is not the case here.[20c,20d]

2.3. Aqueous Suspensions and ^{1}H Relaxometry Properties

Prior to the ^{1}H relaxation measurements, both the pristine MSNs and the Gd-loaded materials were suspended in nanopure water, and the hydrodynamic radiuses of the products were measured by dynamic light scattering (DLS) as shown in **Figure 6**. For 3D Gd-NSMCM-48 samples, all Gd-loaded materials revealed equivalent hydrodynamic diameter distributions,

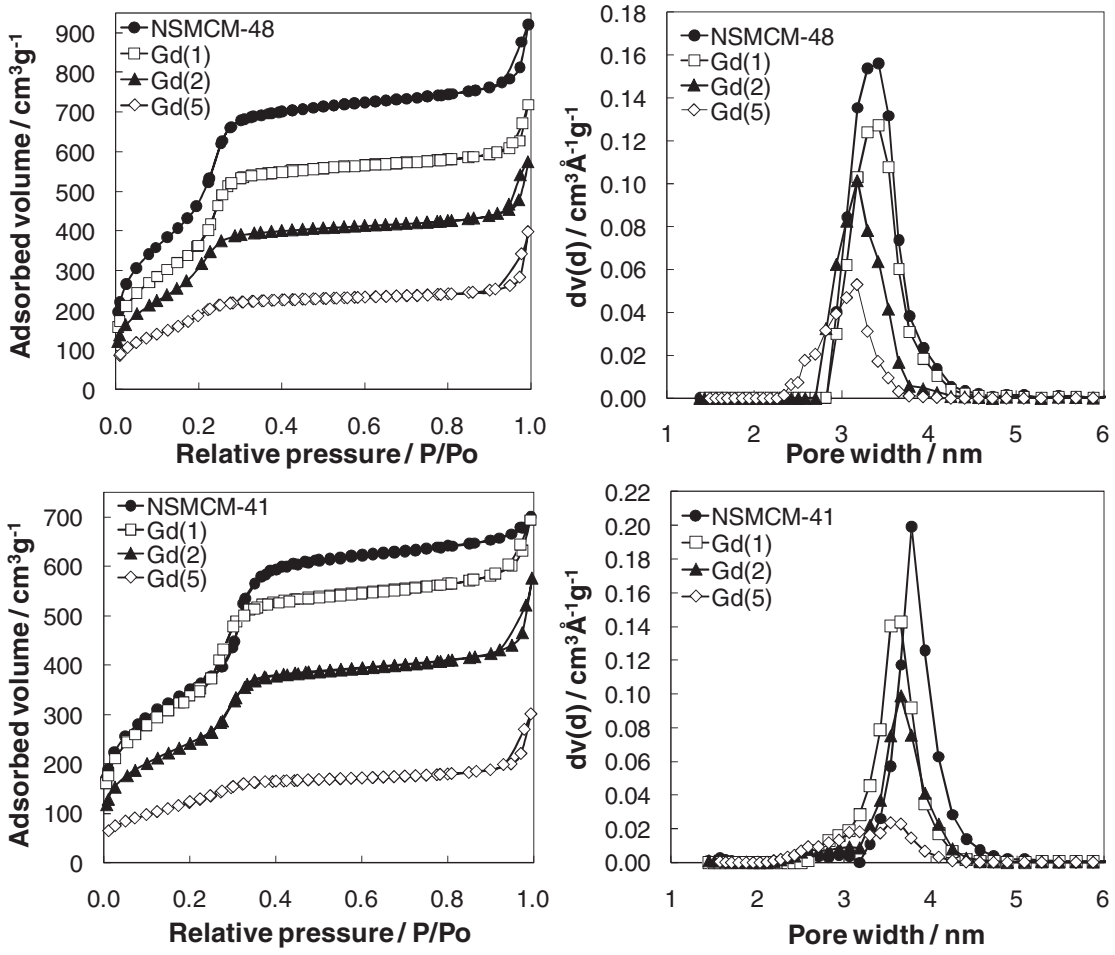

Figure 2. N_2 physisorption isotherms and respective NLDFT pore size distributions of Gd(0,1,2,5)-NSMCM-48 (upper graphs) and Gd(0,1,2,5)-NSMCM-41 (lower graphs).

with a mean value of 174 ± 40 nm (Figure 6b). For 2D Gd-NSMCM-41, slight variations in hydrodynamic diameters occurred depending on the Gd loading, with an average hydrodynamic diameter of 142 ± 50 nm (Figure 6d). Taking into account the hydration corona around the particles, which can represent up to 30% of the hydrodynamic diameter, the particle sizes measured by DLS correlate well with the TEM particle size distributions (Figure S2).

One crucial aspect that had often been neglected in previous studies on Gd-MSNs is the necessity to carefully digest Gd-doped mesoporous silica in aqueous suspensions prior to elemental analysis. As all relaxometric results are normalized to the precise

Table 1. Physicochemical parameters extracted from XRD and nitrogen physisorption measurements.

Sample	BET [m^2g^{-1}]	Pore Vol. [cm^3g^{-1}]	NLDFT des. [nm]	a [nm]	d_s [nm]
NSMCM-48	1601	1.2	3.4	8.0	0.6
Gd(1)-NSMCM-48	1312	0.9	3.4	8.0	0.6
Gd(2)-NSMCM-48	1072	0.7	3.2	7.9	0.8
Gd(5)-NSMCM-48	713	0.4	3.2	7.9	0.8
NSMCM-41	1274	1.0	3.8	4.6	0.8
Gd(1)-NSMCM-41	1244	0.9	3.7	4.5	0.8
Gd(2)-NSMCM-41	886	0.7	3.7	4.5	0.8
Gd(5)-NSMCM-41	454	0.3	3.5	4.5	1.0

The XRD unit cell parameter (a) is equal to $2\,d_{100}/3^{1/2}$ for the hexagonal symmetry and to $6^{1/2}d_{211}$ for the cubic symmetry. The wall thickness (d_s) is evaluated by calculating $d_s = a–DFT_{\text{pore size}}$ for hexagonal symmetry and $d_s = a/2–DFT_{\text{pore size}}$ for cubic symmetry.

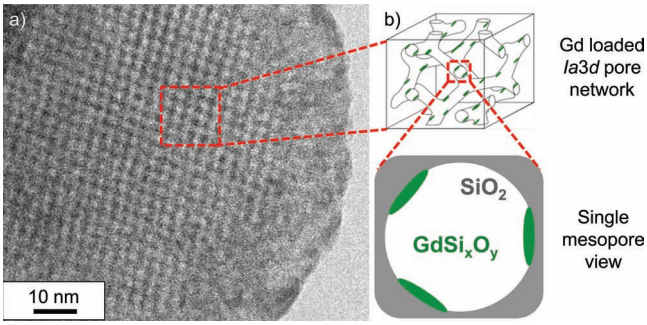

Figure 3. The $GdSi_xO_y$-NSMCM-48 system: a) HRTEM image; and b) schematic representation of the cubic pore network and schematic close-up on a single pore cross-section after insertion of Gd, followed by calcination.

amount of Gd in suspension, the establishment of an optimal digestion procedure includes the use of concentrated HF and HNO_3 prior to inductively coupled plasma mass spectrometry (ICP-MS) quantification, in order to leach all Gd^{3+} ions from the matrix. Then, precise ICP-MS analysis may be performed, allowing the measurement of Gd at ppb detection level, thus enabling exact calculation of proton relaxivity values (**Table 2**). Note that the use of inadequate or less sensitive elemental analysis methods could quickly lead to an underestimation of Gd content and thus to an overestimation of r_1 and r_2 values. As aforementioned, it is necessary to reach relaxometric ratios (r_2/r_1) close to unity for a contrast agent to achieve optimal performance in T_1-weighted imaging. Previously synthesized Gd-MSNs materials have shown relaxometric ratios ranging from 1.48 to 10.9, which were, in general, far from optimal.[4,6] To compare the performance of $GdSi_xO_y$-NSMCM-48 and $GdSi_xO_y$-NSMCM-41 with other systems, the transversal (T_1) and longitudinal (T_2) proton relaxation times of $GdSi_xO_y$-MSNs suspensions were quantified with a dedicated TD-NMR relaxometer, and the Gd ICP-MS measurements were used to plot relaxivity graphs (Figure S4). Relaxivity parameters (r_1, r_2), allowing a direct comparison of the relaxometric performance among contrast agents, were calculated from the slope of these curves (as listed in Table 2).

First, it is obvious from Table 2 that the optimal contrast enhancement effect is not achieved with the highest Gd

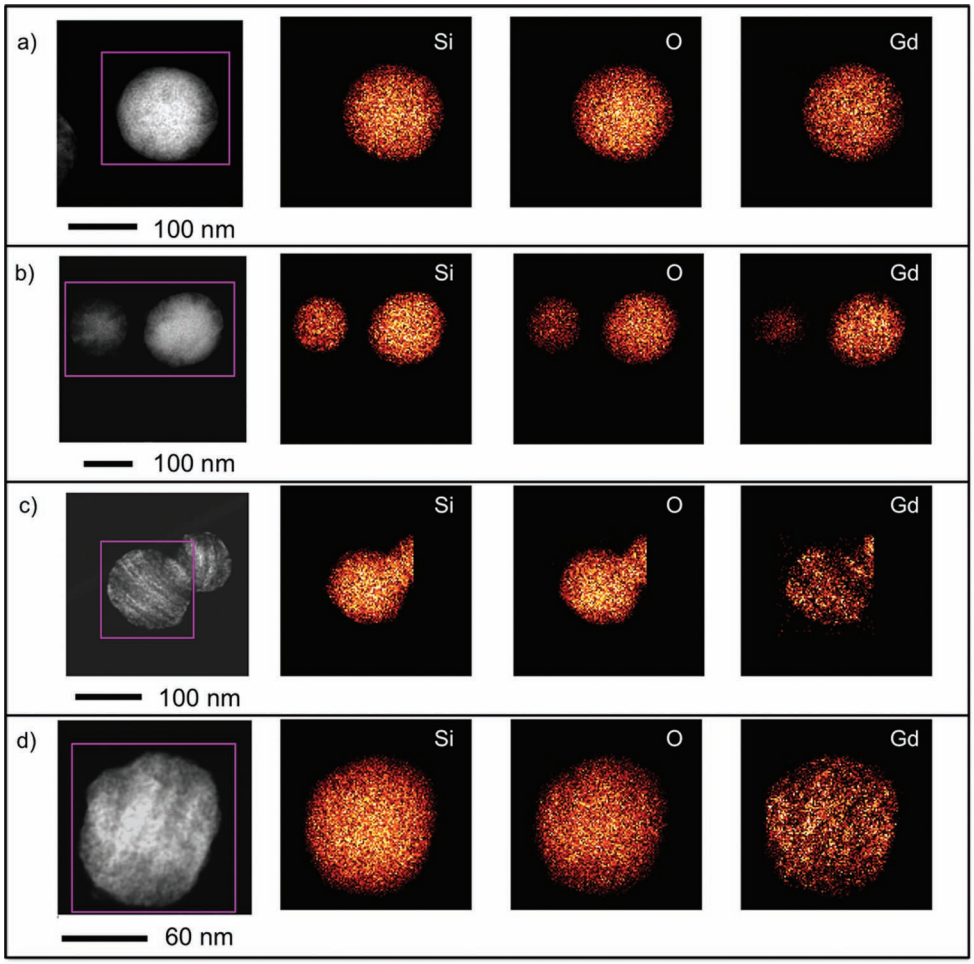

Figure 4. HAADF images of a) Gd(2)-NSMCM-48 and corresponding EDX mapping of silicon, oxygen and gadolinium; b) Gd(5)-NSMCM-48 and corresponding EDX mapping of Si, O and Gd; c) Gd(2)-NSMCM-41 and corresponding EDX mapping of Si, O and Gd; and d) Gd(5)-NSMCM-41 and corresponding EDX mapping of Si, O and Gd.

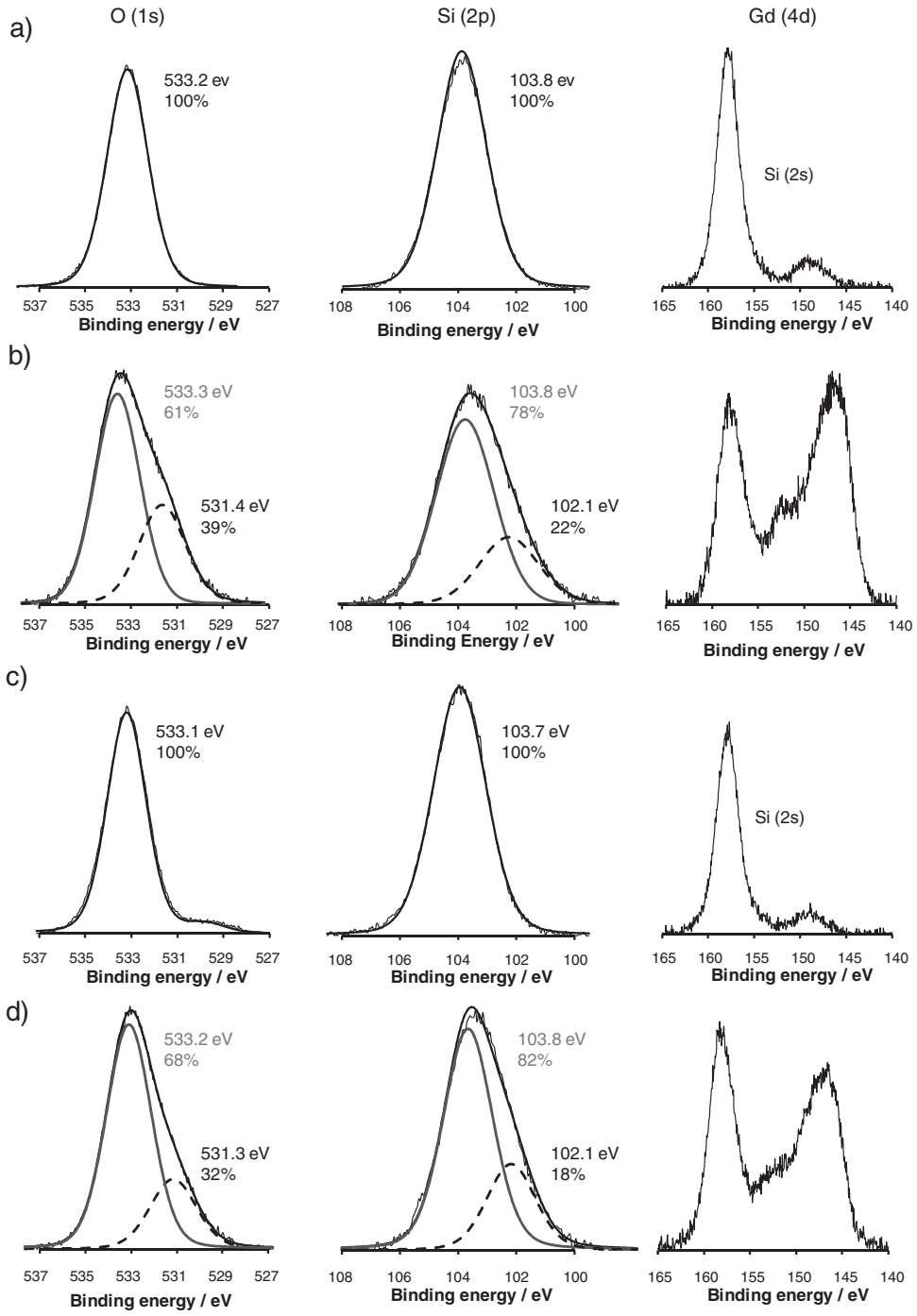

Figure 5. HRXPS spectra of a) NSMCM-48, b) Gd(5)-NSMCM-48, c) NSMCM-41, and d) Gd(5)-NSMCM-41. The solid lines correspond to the total fit.

loading (5 mmol Gd/g SiO_2) but using an intermediate paramagnetic element concentration instead (2 mmol Gd/g SiO_2). Gd(2)-NSMCM-41 and Gd(2)-NSMCM-48 have consistently shown the highest r_1 relaxivities (11.98 and 18.54 $s^{-1}mM^{-1}$, respectively, 3 and 4.6 times higher than Gd-DTPA)[2] and the best r_2/r_1 ratios (≈1.55 in both cases). The fact that Gd(5)-NSMCM-41,48 materials do not show higher r_1 relaxivities could be attributed to a more limited diffusion of water molecules caused by a substantially reduced porosity in these materials (Table 1). Indeed, for Gd(5)-NSMCM-41, specific surface area and pore volume are decreased by 49% and 57%, respectively, as compared to Gd(2)-NSMCM-41, and similar observations are valid for Gd(5)-NSMCM-48. These results are in line with the conclusions formulated by Carniato et al. who, by using Gd-DOTA complexes encapsulated into 2D based MSNs, studied the impact of pore accessibility on the performance of the

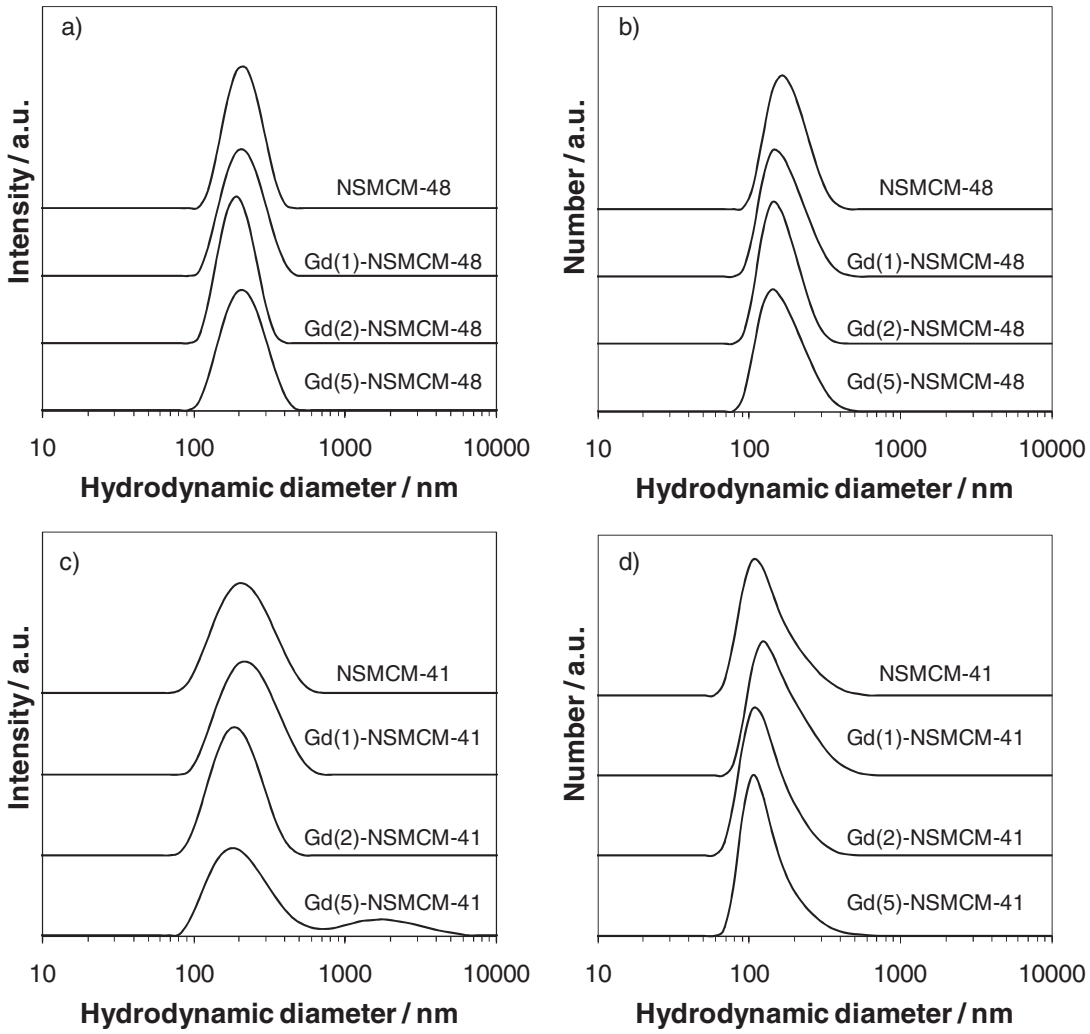

Figure 6. DLS analyses of Gd(*x*)-NSMCM48 samples presented both in a) intensity- and b) number-weighted values; and DLS analyses of Gd(*x*)-NSMCM-41 samples presented both in c) intensity- and d) number-weighted. In all cases, the presented results meet statistical quality criteria, as confirmed by the DLS analysis software (Malvern zetasizer 173°).

material.[7a] In addition, a slight preferential increase in r_2 was noted at higher loadings (5 mmol/g SiO_2) for the 2D product, which could either indicate the presence of thicker paramagnetic coatings, or clusters of paramagnetic atoms in the mesoporous network. Manifestly, a higher loading of gadolinium precursor can be introduced into the pores of MCM-48 MSNs before indication of pore saturation is observed, owing to the higher pore volume and the interconnected nature of this 3D pore network.

In the present study, we have achieved one of the lowest r_2/r_1 ratios reported for all Gd-loaded MSN materials, while demonstrating that grafted Gd^{3+} species are confined inside the mesoporous network. For all of the Gd loadings, the NSMCM-48-based materials provide higher longitudinal relaxometric parameters than the 2D systems and, consequently, could be more effective as contrast agents than their NSMCM-41 counterparts. Indeed, an increased positive contrast can be observed with these materials in T_1 -weighted MRI and at clinical field strength (**Figure 7**) even at very low Gd concentrations, e.g., 0.05 mM. Again, this effect may be explained by the fact that the MCM-48-derived materials exhibit a fully interconnected 3D pore network, which is believed to facilitate diffusion processes.[9]

Importantly, the stability of the aqueous suspension of $GdSi_xO_y$-MSNs was monitored by dynamic light scattering (**Figure 8**). In fact, the colloidal stability of mesoporous silica particles is sporadically discussed in the literature; however, hydrodynamic diameter can affect the relaxometric properties of paramagnetic contrast agents and must be adequately and systematically reported. In our case, no aggregation was observed for at least 48h, and the hydrodynamic diameters of particles remained in agreement with the particle size extracted from TEM. Also, no aggregation or sedimentation was observed during MR imaging, as the contrast remained uniform in the whole of the tube (Figure S5).

Finally, to evaluate the extent of Gd leaching, Gd(2)-MSNs suspensions were dialyzed in a 10 mM saline aqueous media for 7 days (see Experimental section). Noticeable amounts of Gd were

Table 2. Relaxivity parameters (r_1, r_2) in $s^{-1}mM^{-1}$ for $GdSi_xO_y$-MSNs measured in deionized water at 1.5 T and 37 °C ± 1.0.

Sample	Pore network geometry	Dialysis time [h]	r_1 [$s^{-1}mM^{-1}$]	r_2 [$s^{-1}mM^{-1}$]	r_2/r_1
Gd(1)-NSMCM-48	3D	24	7.51	13.87	1.85
Gd(2)-NSMCM-48	3D	24	18.54	28.95	1.56
Gd(5)-NSMCM-48	3D	24	2.58	9.65	3.74
Gd(1)-NSMCM-41	2D	24	7.22	13.88	1.92
Gd(2)-NSMCM-41	2D	24	11.98	18.49	1.54
Gd(5)-NSMCM-41	2D	24	2.48	13.23	5.33

detected by ICP-MS in the saline water batch only during the first 24 h (Figure S6). No further Gd species were then detected in the dialysate solutions for both Gd(2)-NSMCM-48 and Gd(2)-NSMCM-41, even after 6 more days of dialysis. It is important to mention that all MRI images and relaxation parameters shown here were obtained with samples that were dialyzed for 24 h. Thus, these results indicate that the relaxometric measurements of the $GdSi_xO_y$-MSNs particles have been performed after adequate elimination of contaminating Gd^{3+} ions (after 24 h of dialysis). In the perspective of cell monitoring and tracking applications in vivo, the paramagnetic element could also, at a later stage, be introduced in the 3D porous structure using chelates such as DOTA or DTPA. Should evidence of toxicity appear with the $GdSi_xO_y$ system, the much lower cytotoxicity risk associated to Gd^{3+} chelates should guarantee the optimal use of the enhanced relaxometric performance of 3D mesoporous structures demonstrated in this study.

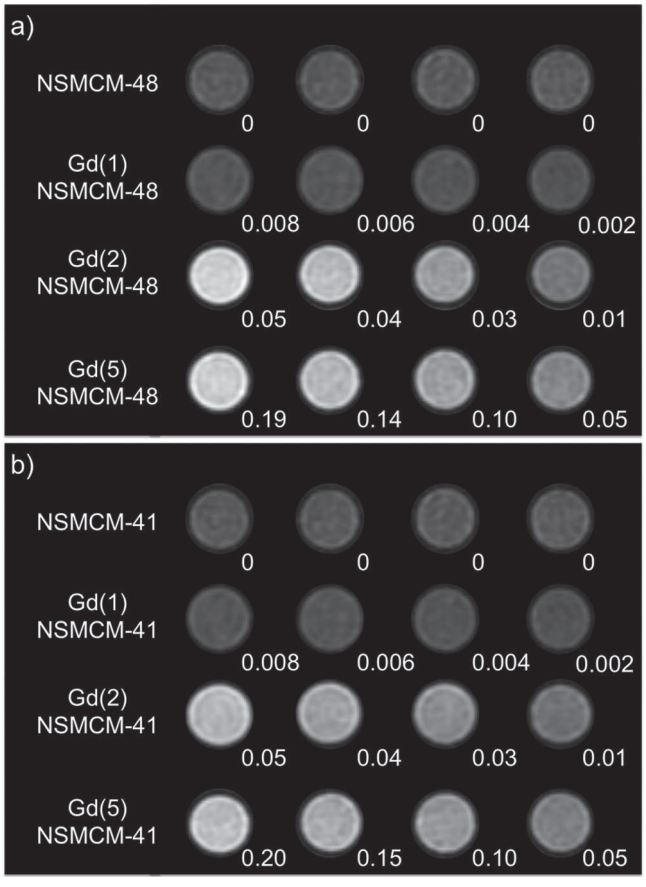

Figure 7. T_1-weighted MR images of a) Gd(*x*)-NSMCM-48 and b) Gd(*x*)-NSMCM-41, measured with a clinical GE Signa 1.5 T system (2D SE, 4 NEX; TE/TR: 10/400 ms; FOV: 11cm; BW: 15.63 kHz, slice thk.: 0.2 cm; 192 × 160; T = 25 °C). Numerical values indicate the Gd concentration (mM) in the imaged solutions, as measured by ICP-MS.

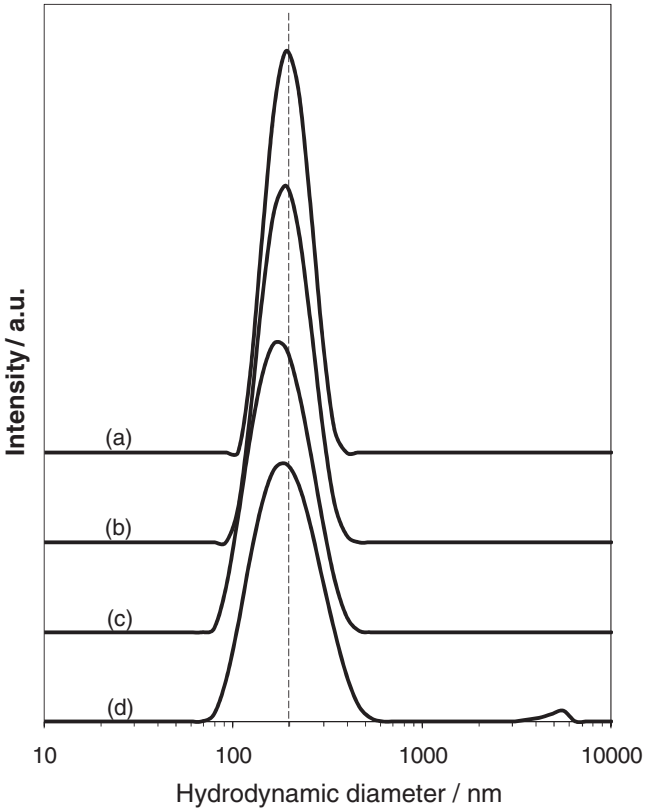

Figure 8. DLS analyses of dialyzed Gd(2)-NSMCM48 aqueous suspension: a) directly after preparation (dotted indicator added as a guiding line), b) after 24 h of dialysis, c) after 24 h of dialysis plus 24 h of static storage at room temperature, and d) after 24 h of dialysis plus 48 h of static storage at room temperature. In all cases, the presented results meet statistical quality criteria, as confirmed by the DLS analysis software (Malvern zetasizer 173°).

3. Conclusions

To summarize, a novel platform based on a 3D mesoporous support and enabling "positive" contrast in T_1 -weighted MR imaging was developed. It is based on the insertion of stable $GdSi_xO_y$ species into mesoporous silica nanoparticles, while maintaining sufficient pore volume. For the first time, a 3D mesoporous network was used to produce a "positive" MR contrast agent, and the relaxometric performances of this system were found to be superior to those of an equivalent 2D pore structure. As such, this study provides a clear illustration of the impact of pore morphology on MR-relaxivity. As a next step, the precise mechanism for the relaxivity enhancement in such 3D mesoporous structures should be investigated further in a dedicated, in-depth relaxometric characterization study. In the present study, longitudinal relaxivities were 4.6 times higher than that of single Gd-DTPA chelates, while maintaining a low r_2/r_1 ratio (1.56). Hence, these 3D $GdSi_xO_y$-MSNs offer an appreciable contrast enhancement at very low Gd concentrations, which could represent a noticeable advantage for more efficient pre-clinical cell labeling and tracking procedures with MRI. Moreover, the 3D mesopore network silica nanoparticles also appear as a very attractive alternative to the currently used 2D equivalent for the development of more powerful MRI contrast agents based on mesoporous materials loaded with Gd chelates.

4. Experimental Section

Materials: Nanospheres with a *3D cubic network* of pores were synthesized by adapting a NSMCM-48 synthesis procedure.[21] In brief, n-cetyltrimethylammonium bromide (1.0 g, CTAB, 99%, Sigma-Aldrich, Canada) and Pluronic F127 (4.0 g, $EO_{106}PO_{70}EO_{106}$, BioReagent, Sigma-Aldrich, Canada) were dissolved in 298 mL of H_2O/NH_3/EtOH [($NH_4OH_{(aq)}$ (2.8 wt%)/EtOH) = 2.5/1 (v/v)]. Then, tetraethylorthosilicate (3.6 g, TEOS, 98% Aldrich, Canada) was added to the solution and vigorously stirred. The reaction mixture was kept 24 h in static conditions (air, RT). The resulting white, solid product was isolated by centrifugation, re-dispersed twice in deionized water (200 mL), isolated again by centrifugation and finally dried overnight in air at 70 °C. Nanospheres with a *2D hexagonal network* of pores were synthesized by adapting a NSMCM-41 synthesis procedure.[10a] In brief, CTAB (1.0 g) was dissolved in deionized water (480 mL), followed by the addition of 2.0 M NaOH aqueous solution (3.5 mL, certified ACS Pellets, Fisher Scientific, Canada). The temperature was adjusted to 80 °C; after 1 h, TEOS (6 mL) was added dropwise to the solution, and the mixture was further stirred for 2 h. The precipitate was then filtered, washed with deionized water, and dried overnight (air, room temperature). Both 3D and 2D MSNs were then calcined at 550 °C for 5 h (air, heating rate 1 °C/min).

Gadolinium ions were subsequently inserted by the incipient wetness technique: in brief, 3D and 2D MSNs (1.0 g each, heated overnight at 150 °C under vacuum) were impregnated with anhydrous EtOH containing 1, 2, and 5 mmol (451.4, 902.8, and 2258 mg) of $Gd(NO_3)_3.6H_2O$ (99.9%, Alfa Aesar). The impregnation required EtOH volumes of 968 µL and 824 µL, corresponding to 80% of the pore volume in each network, respectively (based on physisorption measurements). The materials were then dried overnight (air, 40 °C) and calcined (air, 700 °C, 1 °C/min, 5h). The samples are referred to as Gd(*x*)-NSMCM-48 (3D) and Gd(*x*)-NSMCM-41 (2D), where *x* refers to 1, 2 or 5 mmol of Gd used to impregnate 1 g of each silica template.

Physicochemical characterization: The nanoparticles dispersed in methanol, were deposited on a carbon-coated copper grid, and imaged in TEM (JEM-1230, 80 kV). Particle size distributions were calculated by ImageJ based on a sample of at least 1500 particles, from at least 6 images taken over 6 different quartiles. Both the pore morphology and evidence of Gd distribution in the particles were analyzed by HRTEM (FE-TEM Tecnai G2 F30, 300 kV, KAIST, Korea). Samples were suspended in acetone by ultrasonication. A few droplets of suspended solutions were placed on a carbon micro-grid followed by drying at ambient conditions. High angle annular dark field (HAADF) images and energy dispersive X-ray maps (EDX) were acquired with a FEI Titan 80-300 equipped with image corrector, operated at 300 kV. All the acquisition and data analysis were carried out using Inca EDS system provided by Oxford Instruments (CCEM, Hamilton, Canada). Prior to imaging, samples were prepared by dipping the TEM grid (holey carbon film supported on a copper grid) into the $GdSi_xO_y$-MSNs powders. Nitrogen physisorption measurements (at −196 °C) were performed on outgassed samples (vacuum, 200 °C, >24 h) with an ASAP 2010, Micromeritics. The specific surface area (S_{BET}) was determined using the BET equation in the range $0.05 \geq P/P_0 \geq 0.20$ and the total pore volume was obtained at $P/P_0 = 0.95$. Pore size analysis was completed by using NLDFT methods (Autosorb 1.55 software, Quantachrome Instrument).[22] The NLDFT kernel of equilibrium isotherms was used (i.e., desorption branch, considering N_2 sorption at −196 °C in silica with cylindrical pore geometry). X-ray diffraction (XRD) measurements were performed with a Siemens D5000 (reflection, θ–θ configuration; Cu K_α: $\lambda = 1.541$ Å; 40 kV; 30 mA; 1–55° 2θ, step size: 0.02 2θ, 0.02 s/step). The Jade (v 2.1) software coupled with JCPDS and ICDD (2001 version) databases was used to analyze the XRD data. To assess the binding state of O, Si, C and Gd, X-ray photoelectron spectroscopy (XPS), was performed with a PHI 5600-ci spectrometer (Physical Electronics; Al $K_\alpha = 1486.6$ eV; 300 W; survey spectra in the 1400–0 eV range, with charge neutralization; $\alpha = 45°$; analyzed surface = 0.005 cm^2; pressure < 8.10^{-9} Torr). High resolution analyses were performed on the O (1s), Si (2p) Gd (4d) peaks, and the binding energy scale of the spectra was aligned through the C (1s) peak at 285 eV.

Relaxometric and MRI studies: 5 mg of each Gd(*x*)-NSMCM-48 (3D) and Gd(*x*)-NSMCM-41 (2D) products (*x* = 1, 2, and 5) were dispersed in nanopure water (10 mL; 5 min vortex, 25 min sonication, repeated twice), followed by centrifugation (500 G, 10 min). Finally, the supernatant was dialyzed (1000 MW, Spectra/Por #6, Rancho Dominguez, CA) in nanopure water for 24 h (water changed 4 times, sample-to-volume ratio 1:1000). The hydrodynamic radius of the particles was measured by dynamic light scattering (DLS), using a Malvern DTS Nano zetasizer 173° (equilibration time set to 3 min; 3 measurements taken on each sample; only quality criteria data accepted as valid results). Then, the amount of Gd in the solutions was precisely measured by ICP-MS (Perkin Elmer Elan 6000). Samples of as-dialyzed products were digested in a HNO_3/HF solution: each suspension (200 µL) was diluted in water (800 µL) and put in a Teflon shaft. Then, hydrofluoric acid (0.4 µL, HF 48 wt.%, ACS reagent, Fluka) and HNO_3 (0.3 mL, 69%, ACS reagent, EMD Chemicals) were added and the mixture was heated at 65 °C for 2 h, and left for cooling overnight. The procedure was repeated twice to extract all Gd from the silica matrix prior to ICP-MS. For the Gd retention studies: samples from each one of the Gd(2)-NSMCM-41,48 suspensions (10 mL) were dialyzed (7 days) in 10 mM NaCl saline (1 L). Samples of the dialysate solution (2 mL) were extracted from the saline bath at *t* = 24, 48, 72, 96, 120, 144, 168 h for ICP-MS measurements. The saline solution was refreshed each time. Finally, fractions of as-dialyzed (24h) Gd(*x*)-NSMCM-41 and Gd(*x*)-NSMCM-48 suspensions were distributed in 6.0 mm NMR tubes and diluted with nanopure water (0.05, 0.04, 0.03 and 0.01 mM for *x* = 2). Longitudinal and transversal relaxation times (T_1 and T_2) were measured with a TD-NMR relaxometer (Bruker Minispec 60mq, 60 MHz, 37 °C). Relaxation rates ($1/T_1$ and $1/T_2$) were plotted against Gd concentration values, and relaxivities (r_1 and r_2) were calculated from the slope of these curves. The samples were then imaged with a GE Signa 1.5 T MRI system (nanopure water bowl inserted in a head coil) using T_1-weighted spin-echo sequences (TE: 10 ms; TR: 100, 200, 400, 700, 1000 ms; BW 20; Matrix: 192 × 160; slice thickness: 2 mm; FOV: 110 mm).

Supporting Information

Supporting Information is available from the Wiley Online Library or from the author.

Acknowledgements

The authors acknowledge the financial support from the National Science and Engineering Research Council (Canada), the Canadian Foundation for Innovation and the Fonds québécois de la recherche sur la nature et les technologies (Québec). The authors wish to thank Prof. Ryong Ryoo for access to the high-resolution HRTEM microscope (KAIST, Daejeon, Korea), Dr. C. Andrei and Dr. G. de Silveira at the Canadian Center for Electron Microscopy (CCEM, Hamilton, ON, Canada) for TEM-EDX investigations, and Dr. P. Chevalier (AMSVR-CHUQ and CERMA) for XPS analyses. Supporting Information is available online from Wiley InterScience or from the authors.

Received: July 30, 2011
Published online: October 20, 2011

[1] a) A. S. Arbab, W. Liu, J. A. Frank, *Expert Rev. Med. Dev.* **2006**, *3*, 427; b) R. Weissleder, H. C. Cheng, A. Bogdanova, A. Bogdanov Jr., *J. Magn. Reson. Imaging* **1997**, *7*, 258; c) C. Heyn, C. V. Bowen, B. K. Rutt, P. J. Foster, *Magn. Reson. Med.* **2005**, *53*, 312.

[2] P. Caravan, J. J. Ellison, T. J. McMurry, R. B. Lauffer, *Chem. Rev.* **1999**, *99*, 2293.

[3] J. Kim, H. S. Kim, N. Lee, T. Kim, H. Kim, T. Yu, I. C. Song, W. K. Moon, T. Hyeon, *Angew. Chem. Int. Ed.* **2008**, *47*, 8438.

[4] K. M. L. Taylor, J. S. Kim, W. J. Rieter, H. An, W. Lin, W. Lin, *J. Am. Chem. Soc.* **2008**, *130*, 2154.

[5] B. Julian-Lopez, C. Boissière, C. Chaneac, D. Grosso, S. Vasseur, S. Miraux, E. Duguet, C. Sanchez, *J. Mater. Chem.* **2007**, *17*, 1563.

[6] a) J.-K Hsiao, C.-P. Tsai, T.-H Chung, Y. Hung, M. Yao, H.-M. Liu, C.-Y. Mou, C.-S. Yang, Y.-C. Chen, D.-M. Huang, *Small* **2008**, *4*, 1445; b) C.-P. Tsai, Y. Hung, Y.-H. Chou, D.-M. Huang, J.-K. Hsiao, C. Chang, Y.-C. Chen, C.-Y. Mou, *Small* **2008**, *4*, 186; c) Y.-S. Lin, Y. Hung, J.-K. Su, R. Lee, C. Chang, M.-L. Lin, C.-Y. Mou, *J. Phys. Chem. B* **2004**, *108*, 15608; d) H.-M. Liu, S.-H. Wu, C.-W. Lu, M. Yao, J.-K. Hsiao, Y. Hung, Y.-S. Lin, C.-Y. Mou, C.-S. Yang, D.-M. Huang, Y.-C. Chang, *Small* **2008**, *4*, 619; e) S.-H. Wu, Y.-S. Lin, Y. Hung, Y.-H. Chou, Y.-H. Hsu, C. Chang, C.-Y. Mou, *ChemBioChem* **2008**, *9*, 53.

[7] a) F. Carniato, L. Tei, W. Dastru, L. Marchese, M. Botta, *Chem. Commun.* **2009**, 1246; b) F. Carniato, L. Tei, M. Cossi, L. Marchese, M. Botta, *Chem. Eur. J.* **2010**, *16*, 10727.

[8] J. E. Lee, N. Lee, H. Kim, J. Kim, S. H. Choi, J. H. Kim, T. Kim, I. C. Song, S. P. Park, W. K. Moon, T. Hyeon, *J. Am. Chem. Soc.* **2010**, *132*, 552.

[9] a) T. C. Wei, H. W. Hillhouse, *Langmuir* **2007**, *23*, 5689; b) C. M. A. Parlett, D. W. Bruce, N. S. Hondow, A. F. Lee, K. Wilson, *ACS Catal.* **2011**, *1*, 636.

[10] a) C. Y. Lai, B. G. Trewyn, D. M. Jeftinija, K. Jeftinija, S. Xu, S. Jeftinija, V. S.-Y. Lin, *J. Am. Chem. Soc.* **2003**, *125*, 4451; b) I. I. Slowing, B. G. Trewyn, V. S.-Y. Lin, *J. Am. Chem. Soc.* **2006**, *128*, 14792; c) I. I. Slowing, C.-W. Wu, J. L. Vivero-Escoto, V. S.-Y. Lin, *Small* **2009**, *5*, 57.

[11] J. M. Rosenholm, A. Meinander, E. Peuhu, R. Niemi, J. E. Eriksson, C. Sahlgren, M. Lindén, *ACS Nano* **2009**, *3*, 197.

[12] M. Vallet-Regi, F. Balas, D. Arcos, *Angew. Chem. Int. Ed.* **2007**, *46*, 7548.

[13] W. H. Suh, K. S. Suslick, G. D. Stucky, Y.-H. Suh, *Prog. Neurobiol.* **2009**, *87*, 133.

[14] a) Y.-S. Lin, C.-P. Tsai, H.-Y. Huang, C.-T. Kuo, Y. Hung, D.-M. Huang, Y.-C. Chen, C.-Y. Mou, *Chem. Mater.* **2005**, *17*, 4570; b) D.-M. Huang, Y. Hung, B.-S. Ko, S. C. Hsu, W.-H. Chen, C.-L. Chien, C.-P. Tsai, C.-T. Kuo, J.-C. Kang, C.-S. Yang, C.-Y. Mou, Y.-C. Chen, *FASEB J.* **2005**, *19*, 2014.

[15] S. Giri, B. G. Trewyn, M. P. Stellmaker, V. S.-Y. Lin, *Angew. Chem. Int. Ed.* **2005**, *44*, 5038.

[16] a) H. Vallhov, S. Gabrielsson, M. Stromme, A. Scheynius, A. E. Garcia-Bennett, *Nano Lett.* **2007**, *7*, 3576; b) E. Witasp, N. Kupferschmidt, L. Bengtsson, K. Hultenby, C. Smedman, S. Paulie, A. E. Garcia-Bennett, B. Fadeel, *Tox. Appl. Pharm.* **2009**, *239*, 306.

[17] a) J. Lu, M. Liong, Z. Li, J. I. Zink, F. Tamanoi, *Small* **2010**, *6*, 1794; b) K. O. Yu, C. M. Grabinski, A. M. Schrand, R. C. Murdock, W. Wang, B. Gu, J. J. Schlager, S. M. Hussain, *J. Nanopart. Res.* **2009**, *11*, 15; c) B. G. Trewyn, J. A. Nieweg, Y. Zhao, V. S.-Y. Lin, *Chem. Eng. J.* **2008**, *137*, 23.

[18] V. Alfredsson, M. W. Anderson, T. Oshuna, O. Terasaki, M. Jacob, M. Bojrup, *Chem. Mater.* **1997**, *9*, 2066.

[19] C.-C. Huang, W. Huang, C.-H. Su, C.-N. Feng, W.-S. Kuo, C.-S. Yeh, *Chem. Commun.* **2009**, 3360.

[20] a) G. X. Liu, G. Y. Hong, D. X. Sun, *J. Colloid Interf. Sci.* **2004**, *278*, 133; b) J. A. Gupta, D. Landheer, G. I. Sproule, J. P. McCaffrey, M. J. Graham, K. C. Yang, Z. H. Lu, W. N. Lennard, *Appl. Surf. Sci.* **2001**, *173*, 318; c) W. J. Lademan, A. K. See, L. E. Klebanoff, G. vanderLaan, *Phys. Rev. B* **1996**, *54*, 17191; d) G. vanderLaan, E. Arenholz, E. Navas, A. Bauer, G. Kaindl, *Phys. Rev. B* **1996**, *53*, R5998.

[21] T. W. Kim, P. W. Chung, I. I. Slowing, M. Tsunoda, E. S. Yeung, V. S.-Y. Lin, *Nano Lett.* **2008**, *8*, 3724.

[22] P. L. Ravikovitch, A. V. Neimark, *J. Phys. Chem. B* **2001**, *105*, 6817.